EFFECTS OF SEPTEMBER 5–12, 2017 SOLAR FLARES ON REGIONAL DISTURBANCE OF EARTH'S IONOSPHERE AS RECORDED BY GNSS STATIONS LOCATED IN THE VOLGA FEDERAL DISTRICT OF THE RUSSIAN FEDERATION

D.S. Maksimov (ID)
Kazan (Volga Region) Federal University,
Kazan, Russia, denis-maksimov16@yandex.ru

D.A. Kogogin (ID)
Kazan (Volga Region) Federal University,
Kazan, Russia, denis.kogogin@gmail.com

I.A. Nasyrov (ID)
Kazan (Volga Region) Federal University,
Kazan, Russia, igor.nasyrov@kpfu.ru

R.V. Zagretdinov (ID)
Kazan (Volga Region) Federal University,
Kazan, Renat.Zagretdinov@kpfu.ru

Abstract. The paper presents the results of estimation of the effects of September 5–12, 2017 solar flares on the regional disturbance of Earth's ionosphere according to data from a distributed network of GNSS stations located mostly in the Volga Federal District of the Russian Federation. The GNSS data processing software package we have developed is used to analyze recorded signal power and daily two-frequency phase measurements, as well as to calculate the total electron content and map the data. The results of the study show that during powerful solar flares X2.2 and X9.3 on September 6 the median value of the total electron content, calculated for the Volga Federal District, increased up to 0.25 TECU and 0.6 TECU respectively. At that time, the region of interest (40°–55° E) was sunlit. The pro- longed magnetic storms on September 8 also generated noticeable ionospheric disturbances up to 0.2 TECU. At the same time, neither the solar flares nor the magnetic storms had a significant effect on the power characteristics of the recorded signals from navigation satellites in the region under study. The median carrier-to-noise ratio calculated for the region considered over the entire observation period did not differ from the values recorded under undisturbed ionospheric conditions and varied between 47–53 dBHz and 38–49 dBHz for frequencies $L1$ and $L2$ respectively.

Keywords: ionosphere, GNSS, total electron content, solar flare, magnetic storms, GPS, GLONASS, TEC maps.

INTRODUCTION

Studying wave disturbances in Earth's upper atmosphere is important today because satellite and ground teleradiocommunication systems using transionospheric communication channels are affected by the ionosphere located at altitudes ~50–1500 km above Earth's surface. Free-electron density variations in the ionosphere affect the quality of received signals, thereby leading to an increase in signal delay, a broadening of the Doppler spectrum, as well as an increase in positioning errors.

One of the methods for studying ionospheric plasma is the identification of total electron content (TEC) variations in the ionosphere and the mapping of movement of TEC variations over Earth's surface. For this purpose, dual-frequency phase measurements of signals from Earth navigation satellites (GPS (USA), GLONASS (Russia), Galileo (Europe), Beidou (China)), received by ground-based GNSS stations, are generally carried out.

A fairly large number of papers have studied ionospheric weather by analyzing TEC data for the past three decades. For instance, in [Denisenko, Skazik, 2007; Perevalova, 2014; Laryunin et al., 2014] the following aspects of ionospheric research with the aid of ground GNSS receivers are mentioned: sensitivity, temporal and spatial resolution. It is emphasized that the integral nature of TEC allows us to study mainly horizontal spatial characteristics of ionospheric irregularities. The above works also describe various principles of calculating TEC from GNSS data, using one or two carrier frequencies of signals. Dual-frequency measurements are also divided into two types: with either wave phase difference or signal propagation time. It is noted that phase measurements at two frequencies provide the highest accuracy [Afraimovich, Perevalova, 2006].

The ionosphere is affected by many different factors. One of them is the impact of the Sun in the form of X-ray and ultraviolet radiation, as well as particle fluxes (electrons, protons, and heavy nuclei). Solar flares are classified and detected using the system of geostationary satellites GOES (Geostationary Operational Environmental Satellite) by X-ray flux [Svetska, 1981; GOES I-M Databook, 1996; Syrovatsky et al., 2018]. Levels of solar flares are classified by the peak flux measured in [W/m^2], where the strongest flares are denoted by X and their level exceeds 10^{-4} W/m^2 [https://www.spaceweatherlive.com/ru/pomoshch/chto-predstavlyayut-soboy-solnechnye-vspyshki.html]. X-class flares occur no more than ten times a year and cause a critical level of radio interference on Earth. Problems with radio communication arise due to the complex interaction of solar X-ray and ultraviolet radiation with

Earth's magnetosphere and ionosphere. This interaction gives rise to plasma instabilities, which, in turn, lead to a change in ionization, as well as to frequency, space, and time dispersion of radio signals. All of the above affect a wide range of frequencies of electromagnetic waves (VHF, HF, MF, LF) used in radio communications, ranging, and navigation. Moreover, an increase in ionization causes an increase in TEC [Yasyukevich et al., 2013; Syrovatsky et al., 2018; Qian et al., 2019].

Such studies have not been conducted in the region of interest owing to the low density of GNSS receivers in the Volga Federal District of the Russian Federation. At the same time, the effects of solar flares on ionization of the upper atmosphere are examined regularly by GNSS radio sounding methods with data from the global network of GNSS stations. For example, Syrovatsky et al. [2018] have studied the global effect of solar flares on GNSS signals and have assessed the reliability of their detection in TEC data. Studies were also carried out using GNSS data in automatic mode, taking into account TEC variations. In total, about 4200 receiving stations have been involved. In this paper, 224 solar flares were analyzed from 2014 to 2017. It was shown in particular that during M- and X-class flares on the dayside of Earth TEC increased by 97 % of the background level. The TEC amplitude during the responses varied depending on the class of solar flare and the dynamics of solar ultraviolet and X-ray radiation. It was noted that the automatic classification of solar flares according to TEC data is greatly complicated by the variability of ionospheric response.

Yasyukevich et al. [2018] overview the ionospheric effect of the September 6, 2017 flares by analyzing variations in average global TEC. An increase in the average amplitude of TEC variations to 0.2 TECU on the dayside of Earth was recorded after an X2.2 flare, as well as an increase to 1.3 TECU after an X9.3 flare. At the same time, during the X2.2 flare there was a 30-min threefold increase in the positioning error as compared to the background level. There were no changes recorded in the GNSS signal quality compared to that under quiet space weather conditions.

Qian et al. [2019] have also investigated the global response of TEC variations to the September 6, 2017 X9.3 and September 10, 2017 X8.2 solar flares. The authors managed to figure out that the greatest effects of flares occur at equatorial latitudes. In these spatial regions during the X9.3 flare, TEC variation amplitudes were as high as ~2.5 TECU; and for the latitudes we deal with, ~1 TECU. During the X8.3 flare, the highest amplitudes of TEC variations were up to ~2 TECU, but it is worth noting that the regions where the disturbances were recorded were on the dayside at that time.

In [Afraimovich et al., 2001; Leonovich, 2003], the ionospheric response is shown to depend also on solar flare position. Specifically, it is demonstrated that as the distance between a solar flare and the central solar meridian increases, the intensity of impulsive phase of soft ultraviolet radiation and the TEC response amplitude decrease.

In conjunction with the foregoing and the absence of such studies in the Volga Federal District of the Russian Federation, we have decided to conduct our own analysis. The objective of this paper is to study TEC variations and the power of navigation signals over the Volga Federal District of the Russian Federation during increased solar activity in September 2017. This will fill the existing gap in measurements for this latitude-longitude sector and contribute to improving the accuracy of ionospheric monitoring both regionally and globally. Section 1 presents raw empirical data: the flares that appeared on the Sun during the time period under study, the geomagnetic storms that occurred in Earth's atmosphere, and the format of the data processed in the experiment. Section 2 describes the software package developed with a brief description of stages of processing of GNSS data from a distributed network of base stations. Section 3 analyzes and discuses the results. In conclusion, we draw general conclusions.

1. DESCRIPTION OF THE EXPERIMENT

The initial set of experimental data contains 30-sec GNSS data presented in RINEX 2.10 and 2.11 [Gurtner, 2007] from receiving base GNSS stations (from 70 to 120 depending on the day) for September 5–12, 2017.

It can be seen (Figure 1, *a*) that the GNSS stations employed are mostly concentrated in 40°–60° E, 50°–60° N.

According to [https://www.spaceweatherlive.com/ru/solnechnaya-aktivnost/solnechnyy-cikl.html], there were 49 X-class, 748 M-class, and 7802 C-class flares during solar cycle 24. The most powerful and frequent X-class solar flares occurred in September 2017. From September 5 to September 10, 2017, four X-class and twenty M-class flares were observed. Duration and time of occurrence of the most powerful flares (according to [https://tesis.xras.ru/magnetic_storms.html?m=9&d=8&y=2017]) are shown in Table 1.

During the period of interest, magnetic storms occurred on September 7 and 8, 2017. Particularly noteworthy are two of them: the first one started around 22:00 UTC on September 7 and lasted for ~8 hrs. The second started against the background of the previous one at ~12:00 UTC on September 8 and lasted for ~20 hrs. As an example, Table 2 shows the highest K_p and G indices corresponding to the magnetic storm level [Fleming et al., 1939; https://www.swpc.noaa.gov/noaa-scales-explanation, https://tesis.xras.ru/magnetic_storms.html?m=9&d=8&y=2017], which were recorded from September 5 to 12, 2017. Further, the *Dst* index is also used to analyze the effect of magnetic storms [https://wdc.kugi.kyoto-u.ac.jp/dst_provisional/201709/index.html].
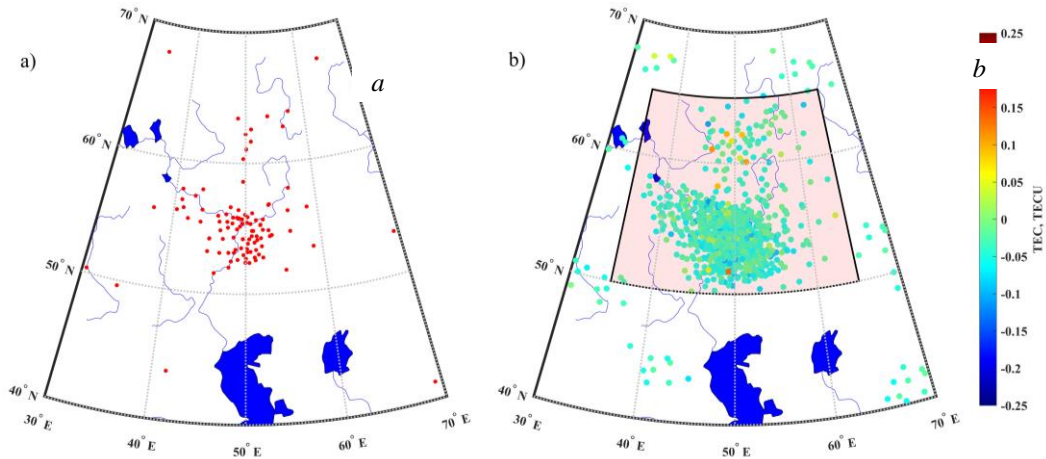
Figure 1. Location of GNSS stations (*a*); a map of the spatial location of the ionospheric pierce points to which TEC variation amplitudes are related (*b*). The highlighted area is the region from which median TEC variations and navigation signal power were calculated

Table 1

Solar flares in September 2017

Date	Flare class	Onset (UTC)	Maximum (UTC)	End (UTC)
September 6	X2.2	08:57:00	09:10:00	09:17:00
September 6	X9.3	11:53:00	12:02:00	12:10:00
September 7	X1.3	14:20:00	14:36:00	14:55:00
September 10	X8.2	15:35:00	16:06:00	15:31:00
September 6	M2.5	15:51:00	15:56:00	16:03:00
September 6	M1.4	19:21:00	19:30:00	19:35:00
September 7	M2.4	04:59:00	05:02:00	05:08:00
September 7	M7.3	10:11:00	10:15:00	10:18:00
September 7	M3.9	23:50:00	23:59:00	00:14:00
September 8	M2.9	18:09:00	18:47:00	19:04:00
September 8	M8.1	07:40:00	07:49:00	07:58:00
September 9	M3.7	10:50:00	11:04:00	11:42:00

Table 2

The highest K_p and G indices on September 5–12, 2017

Date	K_p index	Magnetic storm level	Observation time (UTC)
September 7	8	G4	21:00–00:00*
September 8	8	G4	00:00–03:00
September 8	5	G1	03:00–06:00
September 8	5	G1	09:00–12:00
September 8	8	G4	12:00–15:00
September 8	7	G3	15:00–18:00
September 8	6	G2	18:00–21:00
September 8	5	G1	21:00–00:00*
September 12	5	G1	21:00–00:00*

where 00:00* refers to the start of the next day.

2. METHOD OF EXPERIMENTAL DATA PROCESSING

The overall flowchart for the GNSS data processing algorithm is given in Figure 2. This software package is advanced and adapted to the problems solved in the work; it has been presented in [Kogogin et al., 2020]. Note that the study is based only on GPS and GLONASS satellite data due to the fact that only a small number of base stations, shown in Figure 1, *a*, supported the recording of Galileo and Beidou GNSS signals during the time period considered.

The first stage of the processing is conversion of RINEX files into mat files through MATLAB [https://www.mathworks.com/products/matlab.html]. The conversion is performed for further faster and universal recalculation of TEC data, depending on the
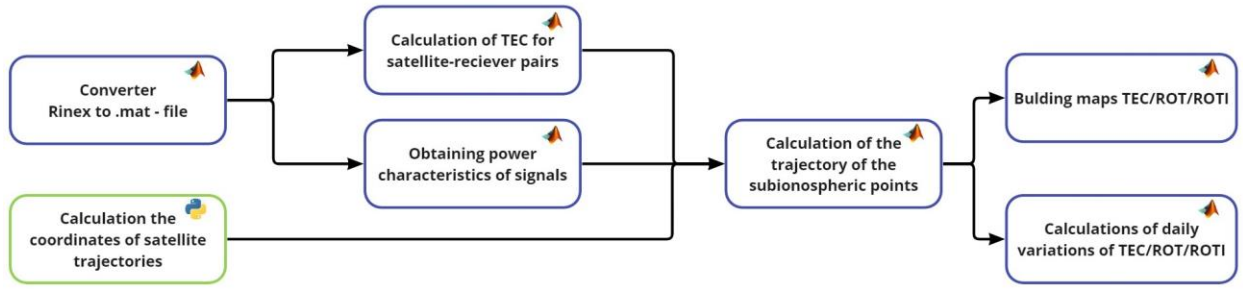
Figure 2. Algorithm of GNSS data processing and TEC calculation

available input parameters, which are identified from the nature of disturbance sources (moving average window, data accumulation time, etc.).

The next step is to calculate slant and vertical TEC from phase measurements at two frequencies [Hofmann-Wellenhof et al., 1994]:

$$I_s = -\frac{1}{K} \frac{f_i^2 f_j^2}{f_i^2 - f_j^2} \Big[\big(L_i \lambda_i - L_j \lambda_j \big) + const + \sigma L \Big], \quad (1)$$

where I_s is slant TEC; K=40.308; $L_i \lambda_i$, $L_j \lambda_j$ are radio signal phase path increments occurring due to phase delay in the ionosphere; $L_i = \dfrac{\Delta \varphi}{2\pi}$ are phase measurements of a GNSS receiver at frequencies f_i; *const* is the ambiguity of phase measurements; σL is the phase measurement error. TECU (Total Electron Content Unit) is utilized as a unit of TEC measurements: 1 TECU=10^{16} el·m^{-2}.

In addition, at this step we remove the trend by subtracting a sixth-degree polynomial from the measurement vector in order to take into account the effect of motion of navigation satellites in orbit. Note that the data acquired at low elevation angles (less than 30°) was excluded from the TEC data in order to obtain more reliable results during the transition from slant TEC to the vertical one:

$$I_v = I_s \cos\left[\arcsin\left(\frac{R_z}{R_E + h_{\max}} \cos\theta_s \right) \right], \quad (2)$$

where I_v is vertical TEC; R_E is the Earth radius [m]; $h_{\max}$ is the height of maximum electron density in the ionospheric F2 layer; θ_s is a navigation satellite's elevation angle.

Parallel to the stage of TEC calculation is the calculation of trajectories of navigation satellites. To do this, a script has been developed in the Python programming language, sending a request with satellite ID, date range, registered user name, and password to the Internet resource Space-track [https://www.space-track.org]. The request is implemented using the Spacetrack library [https://pypi.org/project/spacetrack]. In response to the request, a file in the tle format is created — a two-line data format representing a set of orbit elements for an Earth satellite. Next, using the Skyfield library [https://pypi.org/proje ct/skyfield], we calculate satellite locations at certain time intervals for selected dates. The last step at this stage is to save the calculated values of the satellite trajectories to mat files for further pro-

cessing in MATLAB.

The next step is to determine trajectories of ionospheric pierce points from the equations [Afraimovich, Perevalova, 2006]:

$$\varphi_p = \arcsin\big(\sin\varphi_B \cos\psi_p + \\ + \cos\varphi_B \sin\psi_p \cos\alpha_s \big), \quad (3)$$

$$\lambda_p = \lambda_B + \arcsin\big(\sin\psi_p \sin\alpha_s \sec\varphi_p \big), \quad (4)$$

$$\varphi_p = \frac{\pi}{2} - \theta_s - \arcsin\left(\frac{R_E}{R_E + h_{\max}} \cos\theta_s \right), \quad (5)$$

where R_E is the Earth radius; (φ_p, λ_p) and (φ_B, λ_B) are the geographic coordinates (latitude and longitude) of an ionospheric pierce point and a GNSS receiver respectively; θ_s and α_s are the elevation angle and the azimuth of the line of sight between a GNSS station and a satellite. At the corresponding time points, the TEC variation amplitude is linked to the location of an ionospheric pierce point. Similarly, navigation signal power values (the carrier-to-noise ratio C/N_0) in dBHz, obtained from RINEX files, were linked to the location of the subionospheric point [https://insidegnss.com/measuring-gnss-signal-strength]. Then, we combined the data calculated for one moment of recording by receivers from all lines of sight between GNSS stations and satellites. The interval of the stored processed data files (and hence their maps (see Figure 1, *b*)) is 30 sec since GNSS receivers measured signals once every 30 sec.

One file contained from 500 to 1000 points with TEC variation amplitudes (Figure 1, *b* shows a file with ~800 measurements), as well as 100–150 points with signal power values. A reason for the difference in the number of values of TEC variations and signal power is a fairly small number of receivers capable of recording the navigation signal power parameter. Less than half of the GNSS receivers available recorded power characteristics.

The final data processing stages involved smoothing the vectors by subtracting the moving average with a ten-minute window and the calculation of the change in the median TEC variations and the median power of navigation signals in the region highlighted in Figure 1, *b*.

3. ANALYSIS OF EXPERIMENTAL DATA

In Figures 3–5, blue curves indicate median TEC variations over the Volga Federal District of the Russian

Federation, calculated from GNSS data obtained from receivers located in the spatial region 50°–65° N; 35°–65° E (see Figure 1, *b*), with geomagnetic latitude 42.37°–60.60° and longitude 117.48°–148.11° or 8.2°–22.1°*D* (declination); 67.2°–79.1°*I* (inclination). The calculation was carried out by the IGRF-13 model [Alken et al., 2021]. Each of Figures 3–5 is divided into several horizontal panels representing the days of experiments from September 5 to September 12, 2017.

To assess the effect of solar flares and geomagnetic storms on the quality of radio communications, we recorded a change in the carrier-to-noise ratio C/N_0, corresponding to the signals of the central frequency subbands $L1$ and $L2$ (marked $S1$ and $S2$ in Figures 3–5) received by GNSS stations from navigation satellites. Figure 3–5 present median data values (black solid and black dotted curves respectively) obtained for the spatial region 50°– 65° N; 35°– 65° E. Red, yellow, and blue
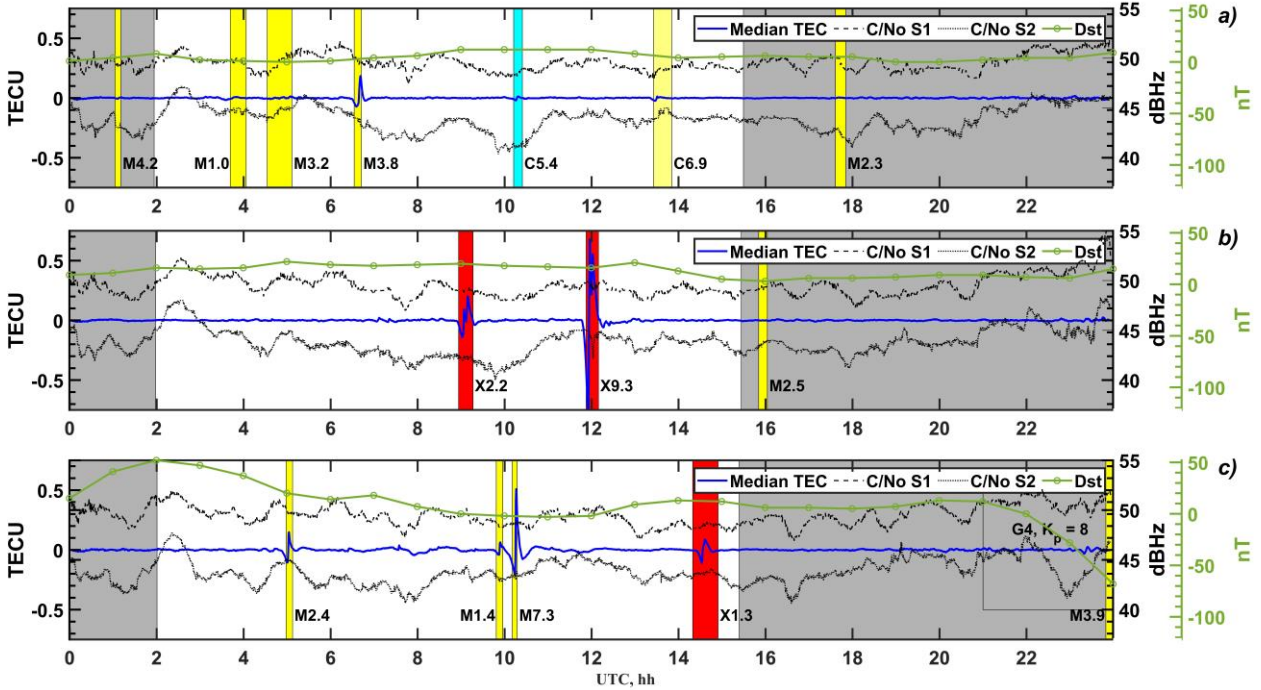
Figure 3. Time variations in median TEC variations (blue curves) and signal power for the frequency $L1$ (black solid curves; $S1$) and for $L2$ (black dotted curves; $S2$); green curves are *Dst* variations. Red, yellow, and blue vertical stripes represent the time intervals of X-, M-, and C-class flares respectively, with estimated flare importance. The transparent rectangle indicates the *G* and K_p indices. The time interval marked with white background corresponds to the daylight hours for Kazan (55.78° N, 49.12° E). Dates of recording: September 5–7 (*a–c*)
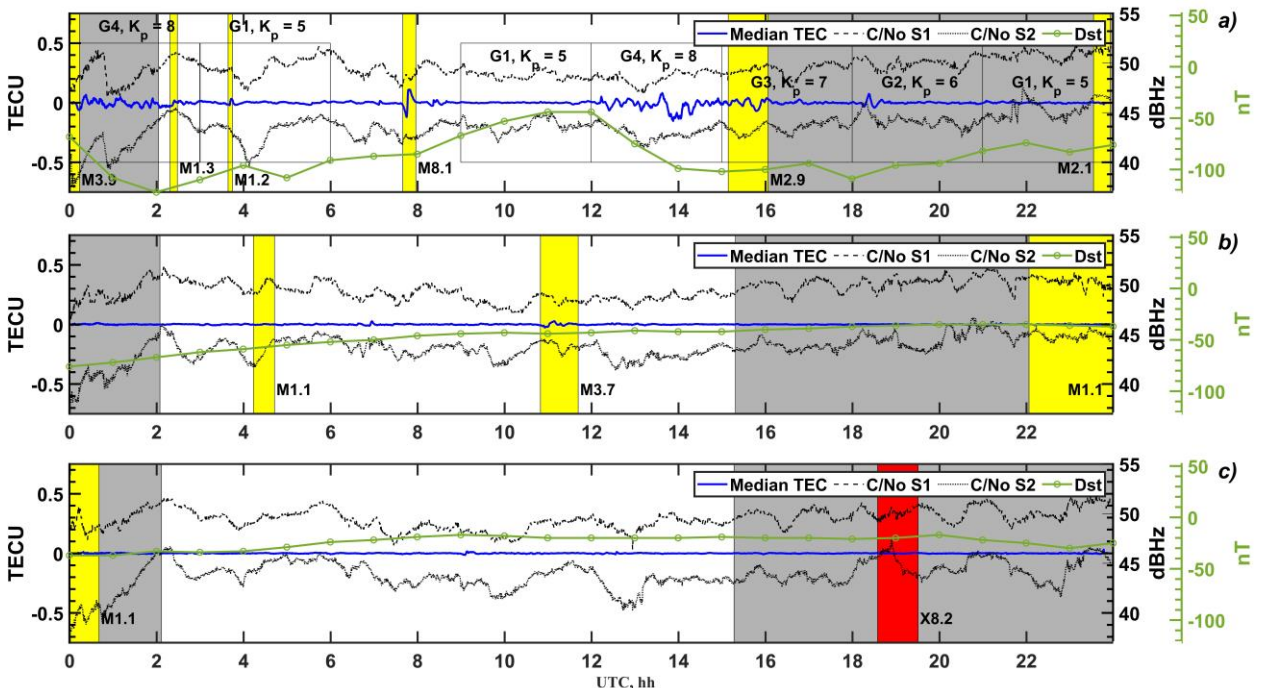

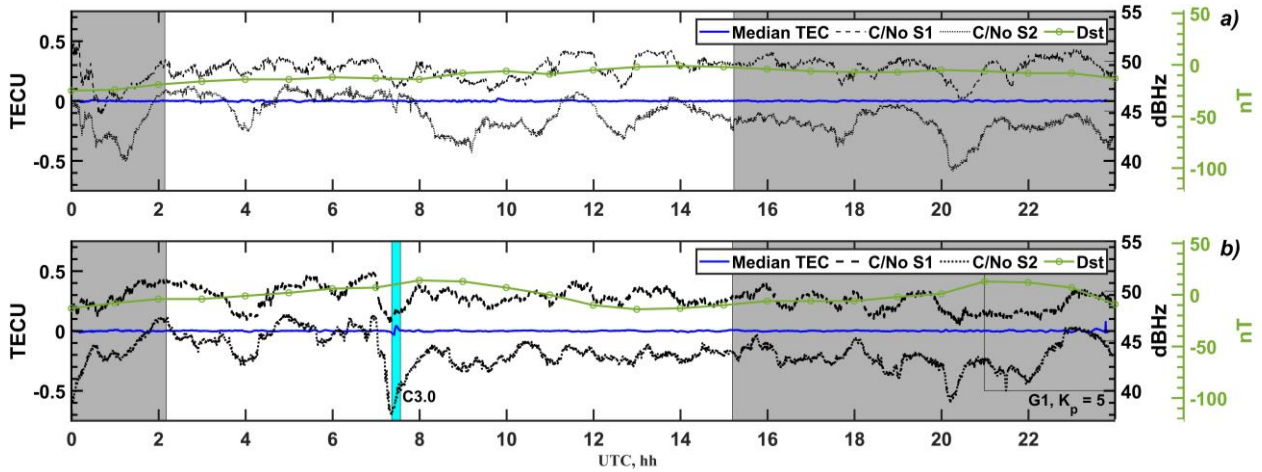*Figure 4*. The same as in Figure 3 for September 8–10, 2017 (*a–c*)

52

Figure 5. The same as in Figure 3 for September 11, 12, 2017 (*a, b*)

rectangles are X-, M-, and C-class flares respectively; transparent rectangles are fixed magnetic storms with given *G* and K_p indices; green curves are *Dst* variations. The white background is the time when the region of interest was on the dayside; the gray background corresponds to the time when it was on the nightside.

The results of experimental data processing show that the most active ionospheric disturbances occurred during the most powerful solar flares (September 6, Figure 3, *b*). The TEC variation amplitude was as high as 0.25 TECU during the X2.2 flare (~9:00 UTC) and 0.6 TECU during the X9.3 flare (~12:00 UTC). It is worth noting that the spatial region 50°–65° N; 35°–65° E under study was on the dayside during the flares. The M7.3 flare on September 7 (see Figure 3, *c*) generated a disturbance up to 0.5 TECU.

Thus, the TEC variations significant relative to background are recorded during the solar flares when the region under study is on the dayside. Note that in the TEC variations there are responses not only to X- and M-class flares, but in some cases to C-class flares too (see Figure 5, *b*).

The longest effects are observed when *Dst*<–50 nT, which is classified as a magnetic storm [Yermolaev, Yermolaev, 2009]: September 7–8 at 23:00–02:00 UTC (see Figures 3, *c*, and 4, *a*) and September 8 at 12:00–16:00 UTC (Figure 4, *a*). In these cases, the amplitude of median TEC variations was as high as 0.2 TECU, but at the same time it had longer-term disturbances (to 3–4 hrs).

From September 5 to 12 in Kazan, sunrise and sunset were from 03:01 to 03:12 and from 15:19 to 15:50 UTC respectively [https://time365.info/voshod-i-zakat-kazan-rossiya]. When the region of interest was on the nightside, the recorded flares, including X-class ones, did not lead to a significant excess of the TEC variation amplitude over the background level. An exception can be considered the post-sunset TEC variations on September 7–8 when geomagnetic storms with K_p=8 and *Dst*<–100 nT occurred.

An important role in the effect of a solar flare on Earth's ionosphere is played by the place of its occurrence on the Sun. The recorded flares were detected in region 2673, which on September 7 and on the following days was on the visible solar limb. If solar flares

were located closer to the central meridian, their effect on Earth's atmosphere would have been stronger [Afraimovich et al., 2001; Leonovich, 2003].

The median carrier-to-noise ratio C/N_0 of navigation signal for *L*1 was ~50 dBHz, for *L*2, 45 dBHz both during solar flares and under quiet heliogeophysical conditions. A decrease in the carrier-to-noise ratio was observed on September 12 at ~06:55–07:20 UTC before the occurrence of a C3.0 flare; it reached 5 dBHz for *L*1 and 10 dBHz for *L*2 in 25 min (see Figure 5, *b*).

CONCLUSION

In the paper, we have estimated the effect of the September 5–12, 2017 solar flares on the ionospheric disturbance level, using proprietary software based on calculated TEC variations and navigation signal power changes. For the analysis, we used GNSS signals received at a distributed network of base stations located mostly in the Volga Federal District of the Russian Federation. In the work, we have tested the software package that performs a full cycle of GNSS data processing, specifically calculations of TEC and its derivatives such as ROT, ROTI, AATR, etc., signal power values, mapping of received data, etc.

After processing the initial dataset, we managed to identify the response of the median TEC variations, calculated for the spatial region 50°–65° N, 35°–65° E, to the effects of X-, M-, and C-class solar flares for all days of research. At the same time, we found out that the flares that occurred after sunset did not significantly change background TEC values for the region under study. It is also worth noting that the powerful geomagnetic disturbances on September 7–8 (see Figures 3, *b* and 4, *a*) caused significant ionospheric disturbances as great as 0.2 TECU lasting for 3–4 hrs. But for a sharp decrease in the carrier-to-noise ratio on September 12, we did not manage to detect a significant decrease in signal power during the days when the solar flares and prolonged magnetic storms occurred.

The data acquired using the original software package was validated according to the results reported in [Yasyukevich et al., 2018; Qian et al., 2019]. We have obtained a good agreement between the results received

on September 06, 2017 for the nature of the TEC variation response to the effects of X2.2 and X9.3 solar flares.

Unfortunately, in this study we were limited to only two constellations of GPS and GLONASS navigation satellites due to the small number of GNSS receivers in the Volga Federal District of the Russian Federation in 2017 capable of recording GNSS data from other constellations of navigation satellites such as Galileo and Beidou. At the moment, in the region of interest (see Figure. 1, *a*), the number of base GNSS receiving stations has increased significantly and most of them can receive signals from all active GNSS constellations. A similar study conducted for the events of current solar cycle 25 can therefore provide more detailed maps of TEC variation intensity distributions, which will increase diagnostic capabilities of this method of examining ionospheric disturbances.

REFERENCES

Afraimovich E.L., Perevalova N.P. GPS Monitoring of the Earth's Upper Atmosphere. Irkutsk, 2006, 479 p. (In Russian).

Afraimovich E.L., Altyntsev A.T., Grechnev V.V., Leonovich L.A. Ionospheric effects of the solares as deduced from global GPS network data. *Adv. Space Res*. 2001, vol. 27, no. 6-7, pp. 1333–1338.

Alken P., Thébault E., Beggan C.D., Amit H., Aubert J., Baerenzung J., Bondar T.N., Brown W.J., et al. International Geomagnetic Reference Field: the thirteenth generation. *Earth, Planets and Space*. 2021, 73, 49. DOI: 10.1186/s40623-020-01288-x.

Denisenko P.F., Skazik A.I. Determination of parameters of moving ionospheric disturbances based on satellite sensing data. *Electromagnetic waves and electronic systems*. 2007, Vol. 12, no. 5, pp. 33–35. (In Russian).

Fleming J.A., Harradon H.D., Joyce J.W. Terrestrial Magnetism and Atmospheric Electricity. Seventh General Assembly of the Association of Terrestrial Magnetism and Electricity at Washington. 1939, Vol. 44, no. 4, pp. 477–478. DOI: 10.1029/TE044i004p00471.

GOES I-M Databook. *Space System Loral*. 1996, p. 184.

Gurtner W. RINEX: The Receiver Independent Exchange Format version 2.11. Astronomical Institute, University of Berne, UNAVXO Boulder, 2007, p. 57.

Hofmann-Wellenhof B., Lichtenegger H., Collins J. Global Positioning System. Theory and Practice, 3rd ed. XIII, Wien, New York: Springer-Velag, 1994, p. 355. DOI: 10.1017/S0016756897438256.

Kogogin D.A., Nasyrov I.A., Shindin A.V., Grach S.M., Maksimov D.S., Zagretdinov R.V., Dementiev V.O. Dynamic changes of the ionospheric artificial airglow region caused by powerful radio emission based on a joint analysis of night-sky snapshots in the 630 nm line and total electron content variation maps. *Radiophysics and Quantum Electronics*. 2020, vol. 63, no. 2, pp. 89–104. (In Russian).

Laryunin O.A., Kurkin V.I., Podlesnyy A.V. Using of data from two closely spaced ionosondes in the diagnosis of moving ionospheric disturbances. *Electromagnetic Waves and Electronic Systems*. 2014, vol. 19, no. 1, pp. 10–17. (In Russian).

Leonovich L.A. Ionospheric response to solar flares and magnetic storms according to the global GPS network: *Abstract of Thesis*. Irkutsk, 2003, 15 p. (In Russian).

Perevalova N.P. Investigation of ionospheric disturbances by the method of trans-ionospheric GPS sensing: *Abstract of Thesis*. Irkutsk, 2014, 32 p. (In Russian).

Qian L., Wang W., Burns A.G., Chamberlin P.C., Coster A., Zhang S.-R., Solomon S.C. Solar flare and geomagnetic storm effects on the thermosphere and ionosphere during 6–11 September 2017. *J. Geophys. Res.: Space Phys*. 2019, vol. 124, iss. 3, pp. 2298–2311. DOI: 10.1029/2018JA 026175.

Svetska Z. Flare observations. Gordon and Breach Science Publisher, 1981.

Syrovatsky S.V., Jasjukevich Ju.V., Vesnin A.M., Edemskij I.K., Voejkov S.V., Zhivet'ev I.V. The influence of solar flares on the Earth's ionosphere in the 24th cycle of solar activity. *Moscow University Physics Bull*. 2018, no. 4, 1840403 p. (In Russian).

Yasyukevich Y.V., Edemskij I.K., Perevalova N.P., Poljakova A.S. Ionosphere response to helio- and geophysical disturbing factors according to GPS data, Irkutsk: ISU Publ., 2013, 271 p. (In Russian).

Yasyukevich Y., Astafyeva E., Padokhin A., et al. The 6 September 2017 X-class solar flares and their impacts on the ionosphere, GNSS, and HF radio wave propagation. *Space Weather*. 2018, vol. 16, iss. 8, pp. 1013–1027. DOI: 10.1029/2018SW001932.

Yermolaev Y.I, Yermolaev M.Y. Solar and interplanetary sources of geomagnetic storms: aspects of space weather. *Geophysical Processes and the Biosphere*. 2009, vol. 8, no. 1, pp. 5–35.

URL: https://wdc.kugi.kyoto-u.ac.jp/dst_provisional/201709/index.html (accessed September 17, 2022).

URL: https://www.spaceweatherlive.com/ru/solnechnaya-aktivnost/solnechnyy-cikl.htm (accessed September 17, 2022).

URL: https://tesis.xras.ru/magnetic_storms.html?m=9&d=8&y=2017 (accessed August 27, 2022).

URL: https://www.swpc.noaa.gov/noaa-scales-explanation (accessed September 25, 2022).

URL: https://www.mathworks.com/products/matlab.html (accessed October 7, 2022).

URL: https://www.space-track.org (accessed October 7, 2022).

URL: https://pypi.org/project/spacetrack (accessed October 7, 2022).

URL: https://pypi.org/project/skyfield (accessed October 7, 2022).

URL: https://insidegnss.com/measuring-gnss-signal-strength (accessed October 23, 2022).

URL: https://time365.info/voshod-i-zakat/kazan-rossiya (accessed January 20, 2023).

URL: https://wdc.kugi.kyoto-u.ac.jp/dst_provisional/201709/index.html (accessed January 20, 2023).

URL: https://rscf.ru/en/project/21-72-00043/ (accessed January 20, 2023).

How to cite this article